Modeling the Bacterial Photosynthetic Reaction Center 3: Interpretation of Effects of Site-Directed Mutagenesis on the Special-Pair Midpoint Potential†

Jeffrey R. Reimers,‡ Jason M. Hughes,§ and Noel S. Hush*,§

School of Chemistry and Department of Biochemistry, University of Sydney, NSW 2006, Australia

Received June 13, 2000; Revised Manuscript Received October 12, 2000

ABSTRACT: Interpretation of changes in midpoint potential of the "special pair" in bacterial photosynthetic reaction centers caused by site-directed mutagenesis is discussed in terms of a simple tight-binding model which relates them to concomitant variations in spin distribution between the two bacteriochlorophyll molecules of the special pair. Our analysis improves on previous similar ones by Allen and co-workers [Artz, K., Williams, J. C., Allen, J. P., Lendzian, F., Rautter, J., and Lubitz, W. (1997) *Proc. Natl. Acad. Sci. U.S.A. 94*, 13582; Ivancich, A., Artz, K., Williams, J. C., Allen, J. P., and Mattioli, T. A. (1998) *Biochemistry 37*, 11812] in that it is both more complete, including electron−phonon coupling, and more accurate. It is applied to analyze data for a series of M160 mutants of *Rhodobacter sphaeroides*, yielding a value of 0.18 ± 0.03 eV for the electronic coupling energy between the highest occupied levels of the two bacteriochlorophylls in the wild-type and a value of the energy offset E_o between the highest occupied molecular orbitals of the L and M bacteriochlorophylls of 0.14 ± 0.03 eV. For a mutant in which the electron hole in the special pair cation is located entirely on the reactive (L) side, a potential of 641 ± 30 mV with respect to the normal hydrogen electrode is predicted. This agrees well with the average value ca. 650 mV observed for the heterodimer mutant HL(M202) in which the bacteriochlorophyll on the unreactive M side has been replaced by a bacteriopheophytin, causing extensive charge localization. However, the deduced coupling is found to be very sensitive to small changes in the assumptions used in the model, and various important chemical effects remain to be included.

Primary charge separation in bacterial photosynthesis occurs at the "special pair", a bacteriochlorophyll dimer P which, on optical excitation, ejects an electron to become the special-pair radical cation P^+. This is the first step in a light-driven redox process which results in transmembrane charge separation. A crucial quantity influencing the speed and efficiency of the reaction is the P/P^+ standard oxidation potential which is usually referenced to the normal hydrogen electrode. Since in practice the potential is measured by redox titration, it is customary to report the midpoint potential, E_m, which is taken to be equal to the standard reduction potential. This is related to the free energy $-\Delta G_0$ of the initial step

$$P^+ + e^- \rightarrow P, \text{ by } \Delta G_0 = -FE_m + FC = -IP \quad (1)$$

where $-C$ is the absolute potential of the reference electrode, F is the Faraday, and IP is the ionization (free) energy of P in the presence of the protein matrix (including water molecules).

A first-principles calculation of the midpoint potential for a particular species is difficult to carry out with sufficient accuracy to be useful in comparing variations from one species to another. While sophisticated computational methods have been applied such as those involving classical electrostatics (*1*) and classical dynamics (*2*), a simpler approach to interpretation is to relate variations in oxidation potential to variations in some other measurable quantity. A series of genetically engineered mutants of *Rhodobacter sphaeroides* has been designed by Allen and co-workers (*3*) explicitly for this purpose, and in this paper, we reanalyze the available experimental data.

The structure of the special pair of the wild-type is shown in Figure 1 [this is based on a recent theoretical structure optimization using a combined quantum-mechanical molecular-mechanical method (*4*), which by refining that determined by X-ray analysis (*5*), provides more accurate values for bond lengths and angles]. The two halves of the special pair are bacteriochlorophyll-*a* molecules which are labeled P_L and P_M. Similarly optimized structures for some of the M160 mutants, as well as many others, are also available (*6*).

Theoretical Model. A simple two-site tight-binding model was introduced by Plato (*7*) and Parson (*8*, *9*) and their co-workers to interpret electronic properties of the special pair. This model has also been applied (as we discuss below) to interpretation of midpoint potentials (*10*, *11*). Here we outline the model; later, we introduce a new, more accurate method for its application; last, we consider its shortcomings in detail, expanding the model to include electron−phonon coupling.

In the model, it is assumed that the solvated highest-occupied molecular-orbital (HOMO)[1] energy levels of P_L and P_M are the only ones which need be directly included and that these are orthogonal and coupled through an interaction

† This work is supported by the Australian Research Council.

* To whom correspondence should be addressed. Phone: 61-2-93514688. Fax: 61-2-93513329. E-mail: hush_n@chem.usyd.edu.au.

‡ School of Chemistry.

§ Department of Biochemistry.

10.1021/bi001341s CCC: $19.00
Published on Web 12/01/2000

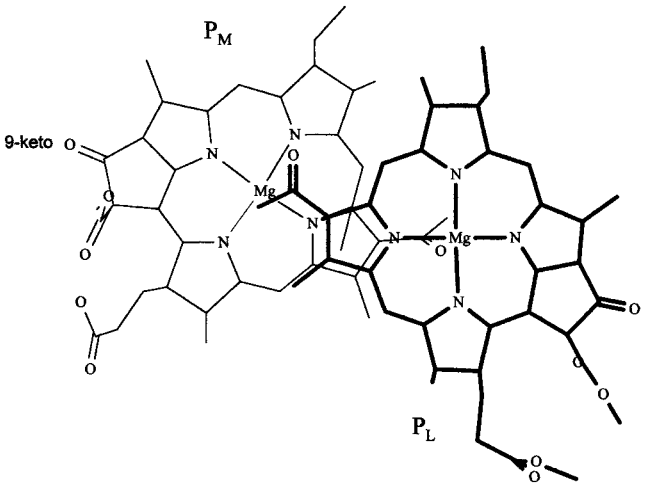

FIGURE 1: Special pair of bacteriochlorophylls from the QM/MM optimized structure (*4*) of the reaction center of *Rb. sphaeroides*, highlighting the 9-keto group of P_M near which the M160 residue lies. The phytyl side chains are not shown.

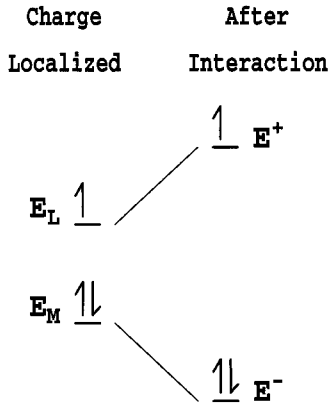

FIGURE 2: Molecular-orbital energy-level scheme for the interacting localized HOMO orbitals of P_L and P_M.

term to yield new orbital energies E^+ and E^- as shown in Figure 2. Further assumptions are that the difference of interaction energies of P and P^+ with the protein matrix is constant over the range of mutants considered and that no internal conformational changes occur as a result of mutation. The electronic Fock matrix, which describes the molecular-orbital energies, then becomes

$$\mathbf{F} = \begin{bmatrix} E_L & \mathrm{J} \\ \mathrm{J} & \mathrm{E_M} \end{bmatrix} \tag{2}$$

where E_L and E_M are the mutation-dependent HOMO energies of each half in the protein but excluding interaction with the other half, and J is the coupling element, assumed to be constant. The midpoint potential of P is evaluated using Koopmans' theorem ($IP = -E^+$) and eq 1 as $E_m = -E^+/F + C$.

The delocalization of charge between the two halves of the dimer results in distribution of spin and charge density between them, and the charge densities are taken to be ρ_L and ρ_M for P_L and P_M, respectively. Two-level models such as eq 2 do not distinguish between spin and charge densities, and experimentally, spin densities are often (*10*) observed through ENDOR or related techniques and taken to represent the charge densities. From the eigenvectors of the Fock matrix, the ratio of the charge densities is given by

$$\frac{\rho_M}{\rho_L} = [(x^2+1)^{1/2} - x]^2 \tag{3}$$

where $x = E_0/(2|J|)$ with $E_0 = E_L - E_M$. Note that if the HOMO orbital on the M half is lower (deeper) in energy than that for the L half, then E_0 and hence x are >0 and ionization occurs preferentially from L so that $\rho_M/\rho_L < 1$. In previous work employing eq 1, an equivalent expression to eq 3 has been reported, but there has been an error in interpretation of the variable. Figures deriving the relationship between the charge ratio and E_o have incorrect x-labels, with, e.g., Figure 7 of ref *12* labeled as "$\Delta\alpha/\beta_D$" ($\Delta\alpha \equiv E_0$, $\beta_D \equiv J$) instead of "$\Delta\alpha/(2\beta_D)$" $\equiv x$. The same problem can be seen explicitly in some written equations, e.g., ref *10*, eq 2, otherwise equivalent to eq 2, above. Our equation may be inverted to give the concise expression

$$\frac{E_0}{|J|} = 2x = \left(\frac{\rho_L}{\rho_M}\right) - \left(\frac{\rho_M}{\rho_L}\right)^{1/2} \tag{4}$$

The midpoint potential E_m can be expressed in a number of ways. One which is most useful for the present purpose relates it linearly to the square root of the ρ_L/ρ_M ratio, with a slope equal to the coupling energy $|J|$ and an intercept corresponding to the midpoint potential for a species in which the hole density in P^+ is located completely on P_L:

$$FE_m = -E_L - |J|\left(\frac{\rho_M}{\rho_L}\right)^{1/2} + FC \tag{5}$$

Application to the M160 Mutant Series of Rb. sphaeroides. Mutants have been designed primarily with the intention of modifying hydrogen-bonding patterns, and correlations between estimated mutation-induced hydrogen bond energy changes and midpoint energies have been proposed (*11*). This is achieved by replacing a wild-type amino acid by another with presumed different ability to hydrogen bond to a carbonyl oxygen center. We discuss one important such set of mutants, namely those obtained by replacing the leucine (Leu) residue at position M160 by another amino acid. The effect on E_m is moderately small; replacement by histidine in the mutant LH(M160) brings about an increase of 57 mV, with the increases for the seven other mutants considered being not as great (*3*, *10*). These changes are attributed predominantly to variations in the strength of hydrogen-bond interaction with the oxygen center of the 9-keto carbonyl group on P_M. This carbonyl group is highlighted in Figure 1.

The M160 mutants all induce changes near the 9-keto group of P_M, directly modifying the localized HOMO energy E_M. As the site of mutation is well removed from P_L, mutation is assumed *not* to alter E_L, however. In Figure 3 and Table 1 the observed (*10*) values of the midpoint potential E_m are shown as a function of $(\rho_M/\rho_L)^2$, with this ratio being approximated by the observed spin-density ratio. A good linear correlation is found with a slope of $|J| = 0.18$

[1] Abbreviations: HOMO, highest occupied molecular orbital; ENDOR, electron nuclear double resonance; Rb, Rhodobacter; QM/MM, quantum mechanics/molecular mechanics; RMS, root-mean-square; PS, photosystem.

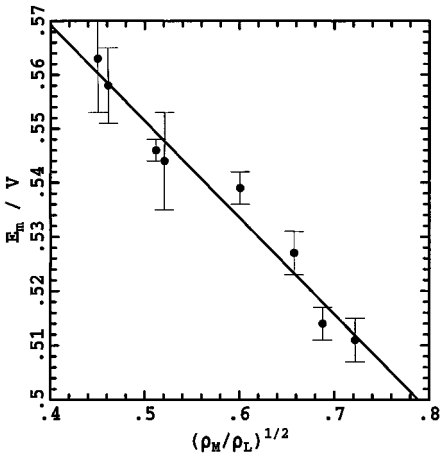

FIGURE 3: Plot of the observed (*10*) midpoint potentials E_m, with error bars, for M160 mutants as a function of the observed charge delocalization indicator $(\rho_M/\rho_L)^{1/2}$ of the radical cation dimer, see eq 5 and Table 1.

eV, intercept $-E_L/F + C$ of 641 mV, and root-mean-square (RMS) deviation of 3 mV. The stated (*10*) uncertainties in the observed E_m data are also shown in Table 1 and Figure 3. Including these, the slope deduced from the figure is actually best represented as $|J| = 0.18 \pm 0.03$ eV.

The deduced coupling J is consistent with the upper bound of $|J| < 0.17$ eV obtained from analysis of the absorption energy of the hole-transfer band (*9*, *13*, *14*) of P^+. Previous interpretations (*10*) of this experimental data, using analytical expressions differing from those given above, led to the conclusion that $|J| = 0.24 \pm 0.04$ eV, which given the available spectroscopic data is clearly unrealistic. However, in the next section, we investigate the sensitivity of the deduced value of $|J|$ to the accuracy of the basic assumptions used in the model and demonstrate that considerable room for improvement still remains.

Within the model, the midpoint potential obtained from the intercept $(\rho_M/\rho_L)^{1/2} = 0$ is $-E_L/F + C = 641$ mV; this is the value expected for a system in which the charge is completely localized on P_L. The heterodimer mutant HL(M202) in which the bacteriochlorophyll P_M is replaced by a pheophytin provides a very good approximation to such a system as experimentally (*15*, *16*) any charge localization on P_M is yet to be detected. Its observed midpoint potential is 650 mV [obtained from the average of observed experimental values (*17*−*19*), which lie in the range 640−660 mV] is in quite good agreement with our intercept of 641 mV. This good agreement is evidence for the reasonableness of the basic assumptions of the model. Using eq 4 and the fitted value of $|J|$, it is possible to determine E_0 for each mutant and hence the value of the charge-localized midpoint potential $-E_M/F + C$, and the results are also shown in Table 1.

From the experimental value (*10*, *11*) of $(\rho_M/\rho_L)^{1/2} = 0.688$ for the wild-type, the value of the orbital-energy difference E_0 in the wild-type is calculated to be 0.136 ± 0.030 eV. The values of the hole-localized midpoint potentials $-E_L/F + C$ and $-E_M/F + C$ consistent with the model are therefore 0.641 and 0.777 ± 0.030 V, respectively, all expressed with respect to the normal hydrogen electrode. Thus, all three parameters (E_L, E_M, and $|J|$) of the model can be deduced consistently from the observed potential data without adjustment.

Chemically, variation in E_M results from the difference between the interaction with the protein of the neutral special pair and the radical cation. It thus embodies the differences between the hydrogen-bond energies of the mutant residues with the 9-keto group of P_M and P_M^+. For hydrogen-bonding mutants, as charge is withdrawn from the 9-keto group during cation formation, the hydrogen-bond strength will be reduced and thus the ionization energy will be increased. The maximum possible increase clearly corresponds to the situation in which the hydrogen bond is completely broken to P_M^+, and this value is simply correspond to the hydrogen-bond energy between neutral P_M and the mutated residue. Also shown in Table 1 are these hydrogen-bond energies ΔH, estimated from the observed (*11*) change $\Delta\nu$ in frequency of the 9-keto group of P_M from the wild-type, as well as $-\Delta E_M$, the change in the deduced ionization potential from that deduced for the wild-type. The observed frequency shifts are also shown in the table, with conversion to ΔH achieved using a Badger-type relation (*20*); a red shift in the CO frequency of 7.0 cm^{-1} occurs for every 1 kcal mol^{-1} of hydrogen-bond strength. Unfortunately, the P_M 9-keto peak is obscured in the strong hydrogen-bonding mutants by more intense modes and hence the experimental values are only approximate. However, from the table an approximate correlation between the localized ionization potential of P_M and the 9-keto hydrogen-bond strength is apparent, supporting the basic validity of the model.

Shortcomings and Extensions of the Model. The basic model includes a number of assumptions, the most important of which are (i) the assumption that the effect of mutations to the 9-keto group of P_M affects only the charge-localized orbital energy E_M but not E_L, (ii) the neglect of electron−phonon coupling, (iii) the assumption that the coupling $|J|$ is not affected by mutation, (iv) the possibility, presented (*21*) by the presence (*22*) of nearby tripdoublet (*23*) states, that the charge densities ρ_L and ρ_M are poorly approximated by the experimental spin densities, and (v) neglect of the effect of strain energy in the protein chain induced by replacement of phenylalanine by smaller amine acids (*6*). Here, we consider the sensitivity of the results obtained to variations in the first two of these assumptions, extending the model to include electron−phonon coupling.

As a large component of the modulation of E_M will be electrostatic in origin and as this is a long-range interaction, some concurrent effect on the L half would be expected. If we assume that the effect on E_L in going from the wild-type to a particular mutant is actually the fraction η of that on E_M, eq 5 can be solved self-consistently to yield E_L for the wild-type and a modified coupling $|J|$; η can then be optimized in order to minimize the RMS deviation. This gives $\eta = -0.023$ (the perceived effect on P_L is thus only 1/40 th of that on P_M), but $|J|$ increases from 0.18 to 0.20 eV. However, the RMS error decreases only trivially in this process and so an accurate value for η cannot be determined. Setting $\eta = 0.05$ results in $|J| = 0.15$ eV. Hence, we see that the deduced value of $|J|$ is very sensitive to assumptions made about the nature of the interaction of P_L with the mutated residue.

The geometrical structures of neutral and cation radical bacteriochlorophyll species differ; thus, as the degree of

Table 1: Observed (*10*) Values of the Midpoint Potential E_m (in V) and the Spin Density Ratio $(\rho_M/\rho_L)^{1/2}$ for Various M160 Mutants of *Rb. sphaeroides*, as well as the Values of the Charge-Localized Midpoint Potential $-E_M/F + C$ of P_M (in V) Deduced from the Model

mutant	E_m	$(\rho_M/\rho_L)^{1/2}$	$-E_M/F + C$	$-\Delta E_M$[a]	$-\Delta H$[b]	$\Delta\upsilon$[c]
LK(M160)	0.511 ± 0.004	0.722	0.759	−0.018	0.000	0
LS(M160)	0.514 ± 0.003	0.688	0.777	0.000	0.093	−15
LN(M160)	0.527 ± 0.004	0.658	0.794	0.017	0.087	−14
LD(M160)	0.539 ± 0.003	0.601	0.830	0.053	∼0.14	∼−23
LQ(M160)	0.544 ± 0.009	0.521	0.890	0.113	∼0.14	∼−23
LE(M160)	0.546 ± 0.002	0.512	0.897	0.120	∼0.14	∼−23
LY(M160)	0.558 ± 0.007	0.461	0.945	0.168	∼0.14	∼−23
LH(M160)	0.563 ± 0.010	0.450	0.956	0.179	∼0.14	∼−23

[a] Change in the fully charge-localized ionization potential (eV) of P_M from that deduced for the wild type. [b] ΔH is the estimated hydrogen-bond energy (eV) of the introduced residue with the 9-keto group of P_M for neutral reaction centers. [c] $\Delta\nu$ is the observed (*11*) shift (cm^{-1}) in the 9-keto frequency of P_M from that in the wild-type.

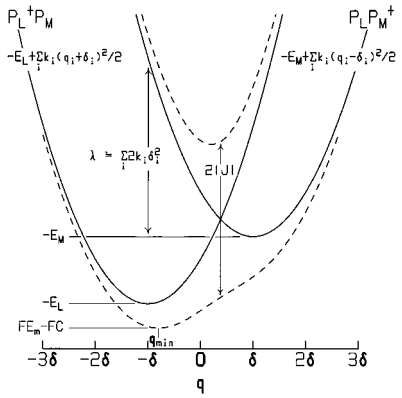

FIGURE 4: Energy surfaces for the localized diabatic electronic states (solid lines) corresponding to $P_L^+P_M$ and $P_LP_M^+$ coupled via the electronic coupling J in **H**(**q**), see eq 6, and the adiabatic states (dashed lines) obtained by diagonalizing this Hamiltonian. The minima of the diabatic states are at $\pm\mathbf{q}$ while the minimum of the lower adiabatic surface is at $\mathbf{q}_{min}$.

charge localization varies, the geometry changes and the associated reorganization energy must be supplied. This electron−phonon coupling has so far been ignored, but the basic model, eq 2, may easily be extended to include this effect. However, while eq 2 depicts the Fock matrix, molecular vibration is more intuitively described in terms of the Hamiltonian matrix **H** describing the energies of the two localized diabatic electronic states $P_L^+P_M$ and $P_LP_M^+$. In the one-electron approximation, $\mathbf{H} = -\mathbf{F}$ and hence the generalized operator is thus

$$\mathbf{H}(\mathbf{q}) = \begin{bmatrix} -E_L + \sum_i \frac{k_i}{2}(q_i + \delta_i)^2 & -J \\ -J & -E_M + \sum_i \frac{k_i}{2}(q_i - \delta_i)^2 \end{bmatrix} \quad (6)$$

where q_i are the antisymmetric vibrational displacements of the dimer away from a configuration of C_2 symmetry for which the force constants are k_i. The minima of these fully localized diabatic surfaces for $P_L^+P_M$ and $P_LP_M^+$ occur at $\mathbf{q} = \delta$ and $\mathbf{q} = -\delta$, with energies (positive) of $-E_L$ and $-E_M$, respectively. They are depicted in Figure 4 and are coupled via the electronic coupling $-J$. In an equivalent representation, this scenario may be described (*24*) in terms of electron−phonon (vibronic) coupling constants and reorganization energies.

Parametrically diagonalizing **H**(**q**) produces adiabatic potential-energy surfaces for the dimer, and these are also shown in Figure 4; specifically, the lower adiabatic surface is given by

$$\epsilon_-(\mathbf{q}) = -E_L + \sum_i \frac{k_i}{2}(q_i + \delta_i)^2 + \frac{E_0(\mathbf{q}) - \{[E_0(\mathbf{q})]^2 + 4J^2\}^{1/2}}{2} \quad (7)$$

where the coordinate-dependent energy difference $E_0(\mathbf{q})$ between the diabatic surfaces is

$$E_0(\mathbf{q}) = -E_M + E_L - \sum_i 2k_i q_i \delta_i \quad (8)$$

The midpoint potential is given by $\epsilon_-(\mathbf{q}_{min})/F + C$, where $\mathbf{q}_{min}$ is the location of the minimum of the lower adiabatic potential-energy surface which, by differentiating eq 9, can be shown to occur when

$$\mathbf{q}_{min} = -\boldsymbol{\delta}\frac{E_0(\mathbf{q}_{min})}{\{[E_0(\mathbf{q}_{min})]^2 + 4J^2\}^{1/2}} \quad (9)$$

Generalizing eq 3, the degree of charge localization is directly obtained from the corresponding eigenvector of **H**(**q**) and is

$$\frac{\rho_M}{\rho_L}(\mathbf{q}) = \left(\frac{\{[E_0(\mathbf{q})]^2 + 4J^2\}^{1/2} - E_0(\mathbf{q})}{2J}\right)^2 \quad (10)$$

so that combining eqs 7−10 leads to

$$FE_m = -E_L + \lambda\rho_M{}^2 - |J|\left(\frac{\rho_M}{\rho_L}\right)^{1/2} + FC \quad (11)$$

where

$$\lambda = \sum_i 2k_i\delta_i{}^2 \quad (12)$$

is the total reorganization energy and $\rho_M \equiv \rho_M(\mathbf{q}_{min})$, etc. Equation 5 may be obtained simply from eq 11 by turning off the electron−phonon coupling, i.e., setting $\lambda = \delta_i = 0$.

The effect of the additional term over the range of data shown in Figure 3 is to modify the slope and add a small amount of curvature. In principle, using eq 11, it is possible to extract the total reorganization energy from the experi-

mental data, but we find that optimization of the value of λ does not lead to a significant reduction in the RMS error and hence this parameter is not obtainable. From the observed (*9*) intervalence absorption band, it is clear that $0 < \lambda < 0.3$ eV and realistic estimates (*24*, *25*) are in the range 0.1 eV $< \lambda <$ 0.2 eV. Constraining $\lambda = 0.1$ eV results in a fitted $|J| = 0.21$ eV, while $\lambda = 0.2$ eV results in $|J| = 0.24$ eV, an unrealistic value. Hence again we see that the value of $|J|$ deduced from the model is very sensitive to assumptions about the nature of the chemical interactions in the system.

CONCLUSIONS

We have revised the application of Allen et al. (*10*, *11*) of the simple tight-binding model of Plato et al. (*7*) and Parson et al. (*8*, *9*) for the interaction of the HOMO levels of P_M and P_L in the special pair of bacterial photosynthetic systems to the interpretation of midpoint potential shifts accompanying mutagenesis. The model has been applied to such interpretation previously (*10*, *11*) but not in a satisfactory way. Specific application of our approach to interpretation of the midpoint changes of the M160 series of mutants has yielded values both for the coupling energy J and for the expected potential for a totally L-localized P^+ system. However, the extracted value of J is found to be very sensitive to the assumptions used concerning the chemical interactions, and extension of the model to include the effects of electron−phonon coupling is found not to improve the fit of the experimental data. Further, we have successfully analyzed (*6*) the midpoint potentials of the heterodimer mutants (in which the effect of intradimer coupling is minimal) using a model in which the most important effect is taken to be the direct electrostatic influence of the mutated residue on P_L. This effect has not been included in the current model.

Both the inclusion of the reorganization energy contribution and direct electrostatic contribution are, of course, required in a complete description of the effect of mutation on the midpoint potential. It is a familiar occurrence in chemistry that a simplified theory is reasonably successful owing to accidental cancellation of effects which have been ignored. Our calculation for the reorganization-energy contribution and exploration of the direct-electrostatic contribution suggest that, here, this is indeed the case. There are a number of additional possibilities such as mutation-dependence of J, spin contamination, and protein strain energy, and these should also be considered in a comprehensive treatment. Work in progress on these microscopic effects includes an a priori treatment of the intermolecular interactions using protein structures calculated (*4*, *6*) by a hybrid quantum-mechanical molecular-mechanical method.

Mutants are now also being produced of the plant photosystems PSI and PSII (see, e.g., refs *26*−*28*), and a key feature of these is the analogous electronic coupling J. In PSII, J is known to be very small, of order 0.01 eV (*29*), and so it will be quite difficult to extract a value for it from electrochemical studies of the effects of mutation such as that of Merry et al. (*26*). Further, effects such as the direct electrostatic influence of the mutated residue on the chromophore and the effects associated with the electron−phonon coupling will be paramount in determining midpoint potentials. It is thus very important that accurate, quantitative models be developed for the simpler case of the midpoint potential of the reaction center in purple bacteria.

REFERENCES

1. Muegge, I., Apostolakis, J., Ermler, U., Fritzsch, G., Lubitz, W., and Knapp, E. W. (1996) *Biochemistry 35*, 8359.
2. Apostolakis, J., Muegge, I., Ermler, U., Fritzsch, G., and Knapp, E. W. (1996) *J. Am. Chem. Soc. 118*, 3743.
3. Lin, X., Murchison, H. A., Nagarajan, V., Parson, W. W., Allen, J. P., and Williams, J. C. (1994) *Proc. Natl. Acad. Sci. U.S.A. 91*, 10265.
4. Hutter, M. C., Hughes, J. M., Reimers, J. R., and Hush, N. S. (1999) *J. Phys. Chem. B 103*, 4906.
5. Ermler, U., Fritzsch, G., Buchanan, S. K., and Michel, H. (1994) *Structure 2*, 925.
6. Hughes, J. M., Hutter, M. C., Reimers, J. R., and Hush, N. S. (2001) Submitted for publication.
7. Plato, M., Lendzian, F., Lubitz, W., and Moebius, K. (1992) *The Photosynthetic Bacterial Reaction Centre II*, Plenum Press, New York.
8. Parson, W. W., Nabedrylk, E., and Breton, J. (1992) in *The photosynthetic bacterial reaction centre II: Structure, spectroscopy and dynamics* (Breton, J., and Vermeglio, A., Eds.) p 79, Plenum Press, New York.
9. Breton, J., Nabedryk, E., and Parson, W. W. (1992) *Biochemistry 31*, 7503.
10. Artz, K., Williams, J. C., Allen, J. P., Lendzian, F., Rautter, J., and Lubitz, W. (1997) *Proc. Natl. Acad. Sci. U.S.A. 94*, 13582.
11. Ivancich, A., Artz, K., Williams, J. C., Allen, J. P., and Mattioli, T. A. (1998) *Biochemistry 37*, 11812.
12. Rautter, J., Lendzian, F., Lubitz, W., Wang, S., and Allen, J. P. (1994) *Biochemistry 33*, 12077.
13. Nabedryk, E., Breton, J., Wachtveitl, J., Gray, K. A., and Oesterhelt, D. (1992) *NATO ASI Ser., Ser. A 237*, 147.
14. Breton, J., Nabedryk, E., and Clerici, A. (1999) *Vib. Spectrosc. 19*, 71.
15. Bylina, E. J., Kolaczkowski, S. V., Norris, J. R., and Youvan, D. C. (1990) *Biochemistry 29*, 6203.
16. Huber, M., Isaacson, R. A., Abresch, E. C., Gaul, D., Schenck, C. C., and Feher, G. (1996) *Biochim. Biophys. Acta 1273*, 108.
17. Davis, D., Dong, A., Caughey, W. S., and Schenck, C. C. (1992) *Biophys. J. 61*, A153.
18. Allen, J. P., Artz, K., Lin, X., Williams, J. C., Ivancich, A., Albouy, D., Mattioli, T. A., Fetsch, A., Kuhn, M., and Lubitz, W. (1996) *Biochemistry 35*, 6612.
19. Laporte, L. L., Palaniappan, V., Davis, D. G., Kirmaier, C., Schenck, C. C., Holten, D., and Bocian, D. F. (1996) *J. Phys. Chem. 100*, 17696.
20. Zadorozhnyi, B. A., and Ishchenko, I. K. (1965) *Opt. Spectrosc. 19*, 306.
21. Reimers, J. R., Hutter, M. C., Hughes, J. M., and Hush, N. S. (2000) *Int. J. Quantum Chem. 80*, 1224.
22. Reimers, J. R., and Hush, N. S. (1995) *J. Am. Chem. Soc. 117*, 1302.
23. Reimers, J. R., and Hush, N. S. (1994) *Inorg. Chim. Acta 226*, 33.
24. Reimers, J. R., and Hush, N. S. (1996) *Chem. Phys. 208*, 177.
25. Reimers, J. R., and Hush, N. S. (1995) *Chem. Phys. 197*, 323.
26. Merry, S. A. P., Nixon, P. J., Barter, M. C., Schilstra, M., Porter, G., and Barber, J. (1998) *Biochemistry 37*, 17439.
27. Mamedov, M. D., Sayre, R. T., and Styring, S. (1998) *Biochemistry 37*, 14245.
28. Semenov, A. Y., Vassiliev, I. R., van der Est, A., Mamedov, M. D., Zybailov, B., Shen, G., Stehlik, D., Diner, B. A., Chitnis, P. R., and Golbeck, J. H. (2000) *J. Biol. Chem. 275*, 23429.
29. Durrant, J. R., Klug, D. R., Kwa, S. L. S., Grondelle, R. v., Porter, G., and Dekker, J. P. (1995) *Proc. Natl. Acad. Sci. U.S.A. 92*, 4798.

BI001341S